PH-UY 2104 Analytical Mechanics Final Project

Armin Ulrich
Instructor: Prof. Gabe Perez-Giz
Code: Git

1 Introduction

In the early 20th century, the German engineer Georg Duffing developed a nonlinear oscillator model while studying the real-world behavior of certain mechanical systems [1]. His original investigations stemmed from efforts to model an *anharmonic* pendulum, where the restoring torque (or force) deviates from the perfectly linear Hookean form ($F = -kx$). A classical pendulum with small oscillations can be approximated by Hooke's law (yielding simple harmonic motion), but for larger deflections, the restoring force becomes intrinsically nonlinear. Duffing sought to capture these higher-order effects and, in doing so, arrived at what is now known as the *Duffing equation*.

Modern research has demonstrated that the Duffing equation captures a broad class of phenomena in mass-spring systems subject to certain nonlinear restoring forces. Specifically, consider a one-dimensional mass-spring oscillator with mass $m = 1$ and a restoring force that includes both linear and cubic terms. The motivation for including a cubic term is rooted in symmetry: if the system's restoring force is symmetric about the origin, the first nonlinear correction to a linear force often appears as a term proportional to x^3 [3]. Hence, the force is expressed as:

$$F(x) \;=\; -kx + \epsilon\, x^3$$

where $k > 0$ is the usual linear spring constant and ϵ is a (usually small) parameter capturing the cubic correction. The emergence of this force from a corresponding *potential energy function* and the conditions under which its shape can produce a *double-well* potential will be examined subsequently.

This project will consider both the *unforced* (no external driving) and *undamped* (no friction or drag) scenarios, as well as the *forced*, *damped* scenarios. Hence, the primary objectives are composed of the following two items:

- **Non-chaotic Duffing regime (undamped & unforced):** Derive the double-well potential, investigate equilibria, analyze the phase portraits, and discuss the exact and perturbative solutions.
- **Chaotic Duffing regime (damped & forced):** Demonstrate how adding damping and periodic forcing can yield complex, even chaotic, motion, visualized through phase portraits and numerical simulations.

2 The Non-Chaotic Duffing Equation

2.1 Deriving the Potential

Consider the restoring force

$$F(x) \;=\; -kx + \epsilon\, x^3 \tag{1}$$

where $k > 0$ is the *linear* spring constant and ϵ is a parameter that governs the strength and sign of the nonlinear (cubic) term. From classical mechanics, the potential energy function $U(x)$ is related to the force via

$$F(x) \;=\; -\frac{dU}{dx}$$

Hence, integrating Eq. (1) with respect to x, the potential energy function is obtained as

$$U(x) \;=\; \int -F(x)\,dx \;=\; \int \left(kx - \epsilon x^3\right) dx \;=\; \frac{1}{2}k\,x^2 \;-\; \frac{1}{4}\epsilon\,x^4 \;+\; C \tag{2}$$

where C is an arbitrary constant of integration that we can just set to 0. Therefore,

$$U(x) \;=\; \frac{k}{2}x^2 \;-\; \frac{\epsilon}{4}x^4 \tag{3}$$

In many physical applications, one sets k as the usual linear stiffness. Thus,

$$U(x) \;=\; \frac{k}{2}\,x^2 \;-\; \frac{\epsilon}{4}x^4$$

2.2 On the Shape of $U(x)$ and "Double-Well" Scenarios

Although Eq. (3) is often described in terms of a "double-well" potential, the precise shape depends on the sign and relative magnitude of ϵ. If $\epsilon > 0$, the quartic term $-\frac{\epsilon}{4}x^4$ eventually dominates for large $|x|$ and drives $U(x) \to -\infty$ as $|x| \to \infty$. Graphically, one sees a concave-down quartic curve that can exhibit local minima away from $x = 0$. In some parameter configurations, those minima are quite pronounced, creating a region reminiscent of a *double well* near moderate $|x|$. However, it is not the traditional stable "two-basin" shape encountered in many references, because at very large $|x|$ the potential goes to negative infinity (an *inverted* scenario essentially). Nevertheless, studying this case still illustrates how a cubic correction to a linear force can produce multiple equilibrium positions in a certain *finite* range of energies.

By contrast, if $\epsilon < 0$, the quartic term $-\frac{\epsilon}{4}x^4$ becomes positive for large $|x|$, so $U(x)$ turns upward at large $|x|$ and yields a more familiar *single-well* shape with steeper boundaries. In that situation, there is only one stable minimum at $x = 0$, consistent with a "hardening" spring.

For completeness, Figure 1 and Figure 2 provide schematic plots of $U(x)$ in these two cases. In the $\epsilon > 0$ case (often called "soft spring"), the potential curve eventually bends downward for large $|x|$. In certain parameter regimes, one can observe local minima separated by a barrier at $x = 0$, but as $|x|$ grows large, $U(x) \to -\infty$. In the $\epsilon < 0$ ("hard spring") case, the potential well becomes increasingly steep as $|x|$ grows, reflecting a greater restoring force than the linear Hookean term alone.

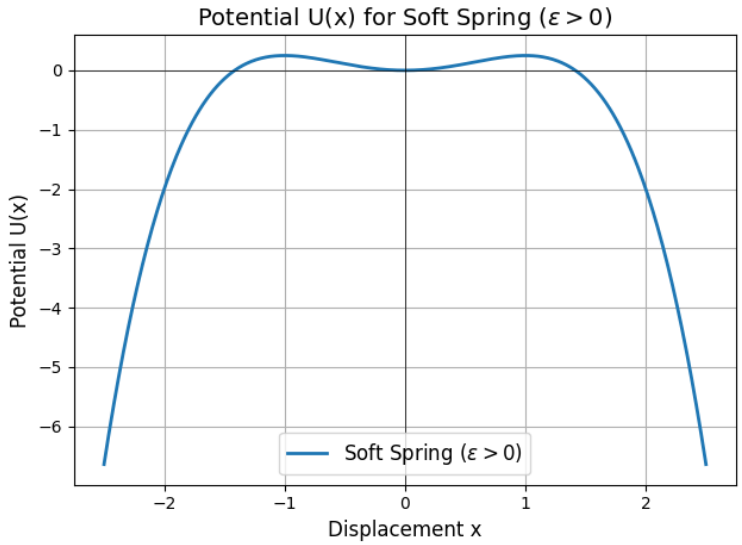

Figure 1: Potential energy $U(x) = \frac{k}{2}x^2 - \frac{\epsilon}{4}x^4$ for $\epsilon > 0$. Although one speaks of a "double-well" near moderate $|x|$, the curve ultimately goes to $-\infty$ as $|x| \to \infty$. This is an *inverted* scenario double well scenario.

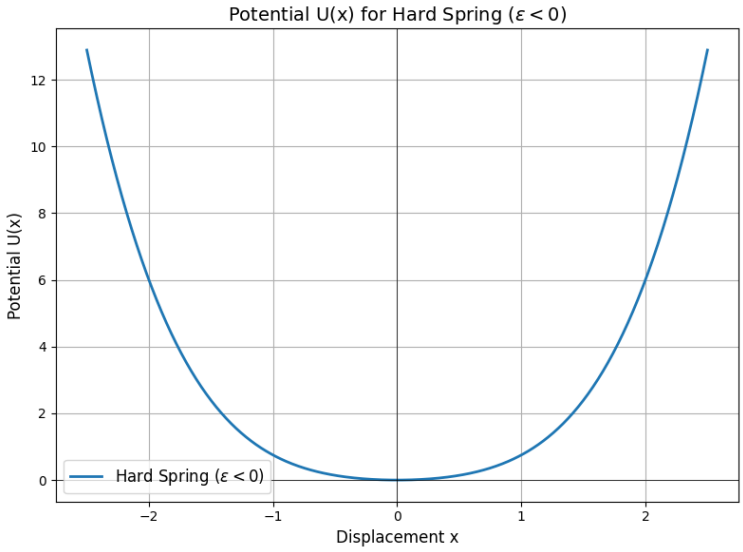

Figure 2: Potential energy $U(x)$ for $\epsilon < 0$ In this "hard spring" regime, the quartic term bends the potential upward at large $|x|$, forming a single stable minimum.

In many treatments [3] of the Duffing equation, one specifically considers cases where $\alpha < 0$ and $\beta > 0$ in the expanded form $(\alpha x^2 + \beta x^4)$ so that the potential is strictly a *stable* double well. By contrast, the $\epsilon > 0$ scenario here can be interpreted as a system with a basin near small $|x|$ but unbounded motion for very large $|x|$. Despite this difference, the local dynamics in the region of interest still provide a rich example of how a cubic correction can yield multiple equilibria and even chaotic behavior under forcing and damping.

Throughout the subsequent sections, the undamped Duffing equation

$$\ddot{x} \; + \; k\,x \; - \; \epsilon\,x^3 \; = \; 0$$

is analyzed. The potential in Eq. (3) encapsulates the interplay of a linear term and a quartic term, with different global shapes depending on ϵ. The local "double-well" or single-well character emerges from how these terms balance for moderate $|x|$, even if the potential ultimately behaves differently at very large amplitude.

3 Duffing Equation and Analysis (Undamped & Undriven)

We now consider the *undamped* and *unforced* Duffing equation:

$$\ddot{x}(t) \; + \; k\,x(t) \; - \; \epsilon\,x^3(t) \; = \; 0, \tag{4}$$

where $k > 0$ (the linear spring constant) and ϵ governs the cubic nonlinearity. We impose initial conditions

$$x(0) \; = \; A, \quad \dot{x}(0) \; = \; 0$$

Where A is the initial displacement from the equilibrium. The goal is to find and compare four solutions/approaches:

1. **Exact (Analytical) Solution via Energy Conservation**
2. **Basic Perturbation Theory**
3. **Poincaré-Lindstedt Method**
4. **Numerical ODE Solver (and Comparison)**

3.1 Exact Solution via Energy Conservation

Since the system is undamped ($\dot{x}$ not multiplied by a friction term) and unforced (no time-dependent external input), the total mechanical energy

$$E \; = \; \tfrac{1}{2}\,\dot{x}^2 \; + \; \left(\,\tfrac{k}{2}\,x^2 \; - \; \tfrac{\epsilon}{4}\,x^4\,\right) \tag{5}$$

remains constant. At $t = 0$, using $x(0) = A$ and $\dot{x}(0) = 0$,

$$E \; = \; \frac{k\,A^2}{2} \; - \; \frac{\epsilon\,A^4}{4}$$

Thus, for any t,

$$\frac{1}{2}\,\dot{x}^2(t) \; + \; \frac{k}{2}\,x^2(t) \; - \; \frac{\epsilon}{4}\,x^4(t) \; = \; \frac{k\,A^2}{2} \; - \; \frac{\epsilon\,A^4}{4} \tag{6}$$

Rearranging to solve for $\dot{x}$:

$$\dot{x} \; = \; \pm\sqrt{k\,A^2 - \epsilon\,A^4 - k\,x^2 + \epsilon\,x^4}$$

Separating variables,

$$\int_A^{x(t)} \frac{d\xi}{\sqrt{k\,A^2 - \epsilon\,A^4 - k\,\xi^2 + \epsilon\,\xi^4}} \; = \; \int_0^t d\tau \tag{7}$$

The integral on the left is an *elliptic integral*, which generally does not reduce to elementary functions. Its solution is typically expressed in terms of *Jacobi elliptic functions* or incomplete elliptic integrals of the first kind. Therefore, the **exact solution** is given implicitly by Eq. (7), though it is quite complicated to write explicitly.

3.2 Basic Perturbation Theory

Suppose ϵ is *small* and consider

$$\ddot{x} + k\,x \;=\; \epsilon\,x^3 \tag{8}$$

We can propose an expansion in powers of ϵ [2]:

$$x(t) \;=\; x_0(t) + \epsilon\,x_1(t) + \epsilon^2\,x_2(t) \;+\; \ldots \quad (\epsilon \ll 1) \tag{9}$$

Step 1: Zeroth-Order (ϵ^0) Equation. At order ϵ^0:

$$\ddot{x}_0 + k\,x_0 = 0$$

The solution to this standard harmonic oscillator is

$$x_0(t) \;=\; A_0\cos\big(\omega t\big) + B_0\sin\big(\omega t\big), \quad \omega = \sqrt{k}$$

From the initial conditions $x(0) = A$ and $\dot{x}(0) = 0$, we get $A_0 = A$ and $B_0 = 0$. Thus

$$x_0(t) \;=\; A\,\cos(\omega t)$$

Step 2: First-Order (ϵ^1) Equation. Substituting $x = x_0 + \epsilon\,x_1$ into Eq. (8), we collect terms of order ϵ^1. Noting that $\ddot{x} = \ddot{x}_0 + \epsilon\,\ddot{x}_1$ and $x^3 = (x_0 + \epsilon\,x_1)^3 \approx x_0^3$ at first order, we obtain:

$$\ddot{x}_1 + k\,x_1 \;=\; x_0^3(t) \tag{10}$$

We already know $x_0(t) = A\cos(\omega t)$. Hence

$$x_0^3(t) \;=\; A^3\,\cos^3(\omega t) \tag{11}$$

Recall the trigonometric identity:

$$\cos^3(\theta) \;=\; \frac{3\cos(\theta) + \cos(3\theta)}{4}$$

Therefore,

$$x_0^3(t) \;=\; A^3\left[\frac{3\cos(\omega t) + \cos(3\omega t)}{4}\right] \;=\; \frac{3A^3}{4}\,\cos(\omega t) \;+\; \frac{A^3}{4}\,\cos\big(3\omega t\big)$$

Thus Eq. (10) becomes

$$\ddot{x}_1 + k\,x_1 \;=\; \frac{3A^3}{4}\,\cos(\omega t) \;+\; \frac{A^3}{4}\,\cos(3\omega t). \tag{12}$$

We solve this inhomogeneous ODE by looking for particular solutions. The homogeneous solution is $x_{1,\mathrm{hom}}(t) = C_1\cos(\omega t) + C_2\sin(\omega t)$, but we set those constants based on boundary/orthogonality considerations soon.

Step 3: Particular Solution—Non-Resonant Term. The $\cos(3\omega t)$ part is *non-resonant*, because the driving frequency 3ω is not equal to the natural frequency ω. We can guess a particular solution of the form

$$x_{1,\mathrm{p1}}(t) \;=\; \alpha\cos(3\omega t) + \beta\sin(3\omega t)$$

Substitute into $\ddot{x}_1 + k\,x_1$ We use:

$$\ddot{x}_{1,\mathrm{p1}} = -9\omega^2\,\alpha\,\cos(3\omega t) - 9\omega^2\,\beta\,\sin(3\omega t),$$

and recall $k = \omega^2$. So

$$(\ddot{x}_{1,\mathrm{p1}} + k\,x_{1,\mathrm{p1}}) = (-9\omega^2+\omega^2)\alpha\,\cos(3\omega t) + (-9\omega^2+\omega^2)\beta\,\sin(3\omega t) = -8\omega^2\left[\alpha\cos(3\omega t) + \beta\sin(3\omega t)\right]$$

We want this to equal $\frac{A^3}{4}\cos(3\omega t)$. Hence we match coefficients:

$$-8\,\omega^2\,\alpha = \frac{A^3}{4}, \quad -8\,\omega^2\,\beta = 0$$

Thus

$$\alpha = -\,\frac{A^3}{32\,\omega^2}, \quad \beta = 0$$

Hence the particular solution for the $\cos(3\omega t)$ part is

$$x_{1,\mathrm{p1}}(t) \;=\; -\,\frac{A^3}{32\,\omega^2}\,\cos(3\omega t)$$

Step 4: Particular Solution—Resonant Term. The $\cos(\omega t)$ part is *resonant*, because the forcing frequency ω matches the natural frequency of the homogeneous solution. A standard ansatz for a resonant term is

$$x_{1,\mathrm{p2}}(t) \;=\; t\left[a\,\sin(\omega t)\right]$$

(We do *not* guess $\cos(\omega t)$ or $\sin(\omega t)$ alone because that conflicts with the homogeneous solution and fails to solve the inhomogeneous problem in the presence of resonance.) Let us compute:

$$x_{1,\mathrm{p2}}(t) = a\,t\,\sin(\omega t)$$

Then

$$\dot{x}_{1,\mathrm{p2}} = a\,\sin(\omega t) + a\,\omega\,t\,\cos(\omega t),$$
$$\ddot{x}_{1,\mathrm{p2}} = 2\,a\,\omega\,\cos(\omega t) - a\,\omega^2\,t\,\sin(\omega t)$$

Substitute into LHS of $\ddot{x}_1 + k\,x_1 = \frac{3A^3}{4}\,\cos(\omega t)$:

$$\ddot{x}_{1,\mathrm{p2}} + k\,x_{1,\mathrm{p2}} = \big(2\,a\,\omega\,\cos(\omega t) - a\,\omega^2\,t\,\sin(\omega t)\big) \;+\; \omega^2\,\big(a\,t\,\sin(\omega t)\big).$$

Notice the last two terms cancel:

$$-\,a\,\omega^2\,t\,\sin(\omega t) \;+\; \omega^2\,a\,t\,\sin(\omega t) = 0$$

Hence we are left with

$$2\,a\,\omega\,\cos(\omega t)$$

We want this to match the forcing $\frac{3A^3}{4}\,\cos(\omega t)$. Thus

$$2\,a\,\omega = \frac{3\,A^3}{4} \quad\Longrightarrow\quad a = \frac{3\,A^3}{8\,\omega}$$

Hence the resonant particular solution is

$$x_{1,\mathrm{p2}}(t) \;=\; \frac{3\,A^3}{8\,\omega}\,t\,\sin(\omega t)$$

Step 5: Combine and Apply Initial Conditions. Collecting the two parts, the full particular solution at $\mathcal{O}(\epsilon)$ is:

$$x_{1,\mathrm{p}}(t) \;=\; -\,\frac{A^3}{32\,\omega^2}\,\cos(3\omega t) \;+\; \frac{3\,A^3}{8\,\omega}\,t\,\sin(\omega t)$$

Then the **first-order** solution becomes

$$x(t) \;\approx\; x_0(t) + \epsilon\,x_{1,\mathrm{p}}(t) \;=\; A\,\cos(\omega t) \;+\; \epsilon\left[-\,\frac{A^3}{32\,\omega^2}\,\cos(3\omega t) \;+\; \frac{3\,A^3}{8\,\omega}\,t\,\sin(\omega t)\right]$$

Because of the $t\,\sin(\omega t)$ term, this solution *secularly* grows with t. Thus for large t (or more specifically when $t \gg \frac{1}{\epsilon}$), it drifts away from the true bounded oscillation. This exemplifies why *basic perturbation theory* fails for long times.

3.3 Poincaré-Lindstedt Method

The idea here is to try to *renormalize* the frequency so that no resonance term appears at first order, removing the secular growth. We rewrite time as

$$\tau \;=\; \Omega\,t, \tag{13}$$

where Ω is an *unknown* frequency we expand in powers of ϵ. Specifically:

$$\Omega \;=\; \omega + \epsilon\,\Omega_1 + \epsilon^2\,\Omega_2 + \cdots, \quad \omega = \sqrt{k}$$

We then write the solution as

$$x(t) \;=\; X(\tau) \;=\; X\big(\Omega\,t\big).$$

Hence

$$\dot{x} = \frac{dX}{dt} = \Omega\,\frac{dX}{d\tau}, \quad \ddot{x} = \Omega^2\,\frac{d^2X}{d\tau^2}$$

Substitute into $\ddot{x} + k\,x - \epsilon\,x^3 = 0$:

$$\Omega^2\,\frac{d^2X}{d\tau^2} \;+\; k\,X \;-\; \epsilon\,X^3 \;=\; 0$$

Group by powers of ϵ. At $\mathcal{O}(\epsilon^0)$, we temporarily set $\Omega^2 = k$. That is, $\Omega = \omega$ at zeroth order. Hence

$$k\,X_0''(\tau) + k\,X_0(\tau) = 0 \;\;\Longrightarrow\;\; X_0''(\tau) + X_0(\tau) = 0 \tag{14}$$

The general solution is

$$X_0(\tau) = A\,\cos(\tau) + B\,\sin(\tau)$$

From initial conditions $X_0(0) = A$ and $\dot{X}_0(0) = 0$, we deduce $B = 0$. (One must also translate $\dot{X}_0(0)$ carefully, but effectively we want $X'(0) = 0$ in τ-units) So

$$X_0(\tau) = A\,\cos(\tau).$$

Next, at $\mathcal{O}(\epsilon^1)$, we must include the correction to Ω Write

$$\Omega^2 = (\omega + \epsilon\,\Omega_1 + \dots)^2 = \omega^2 + 2\,\omega\,\epsilon\,\Omega_1 + \cdots = k + 2\,\omega\,\epsilon\,\Omega_1 + \dots$$

since $\omega^2 = k$. The first-order equation becomes

$$\big(k + 2\,\omega\,\epsilon\,\Omega_1\big)\,X_1''(\tau) \;+\; k\,X_1(\tau) \;-\; \epsilon\,X_0^3(\tau) = 0$$

More systematically, one can rearrange so that the solvability condition ensures no $\cos(\tau)$ resonance occurs. After some algebra (see Appendix Section A.1), it can be shown that the required condition for no secular term (by a comparison of coefficients) leads to

$$\Omega_1 = \frac{3\,A^2}{8}$$

Hence the frequency Ω is:

$$\Omega = \omega + \epsilon\,\frac{3\,A^2}{8} + \cdots$$

For a *first-order* approximation, we then write:

$$x_{\mathrm{PL}}(t) = X_0\big(\Omega\,t\big) \;=\; A\,\cos\Big[\big(\omega + \epsilon\,\tfrac{3\,A^2}{8}\big)\,t\Big]$$

No secular (time×sin) term appears, and the oscillation remains bounded for all t. This is the essence of the Poincaré-Lindstedt technique: **adjust the frequency to absorb the resonance** at each order in ϵ.

3.4 Numerical ODE Solver, Phase Diagram, and Extended Observations

A common strategy for obtaining a numerical solution to the Duffing equation is to employ a Runge–Kutta (RK) method. It is an algorithm that iteratively uses multiple function evaluations within each time step to approximate the solution of ordinary differential equations with high accuracy. The second-order Duffing equation

$$\ddot{x}(t) + k\,x(t) - \epsilon\,x^3(t) = 0$$

is recast as a set of coupled first-order equations by introducing the velocity $v = \dot{x}$, leading to

$$\dot{x} = v, \quad \dot{v} = -\,k\,x \;+\; \epsilon\,x^3$$

An adaptive Runge–Kutta method, such as the RK45 algorithm, can then be applied to integrate forward in time from the initial conditions $x(0) = A$ and $v(0) = 0$. This procedure naturally handles the nonlinear term $\epsilon\,x^3$ without requiring linearization and adaptively refines the time-step size where needed for improved accuracy. The outcome is a time series $\big(x(t), v(t)\big)$ that serves as a reference solution for moderate values of ϵ.

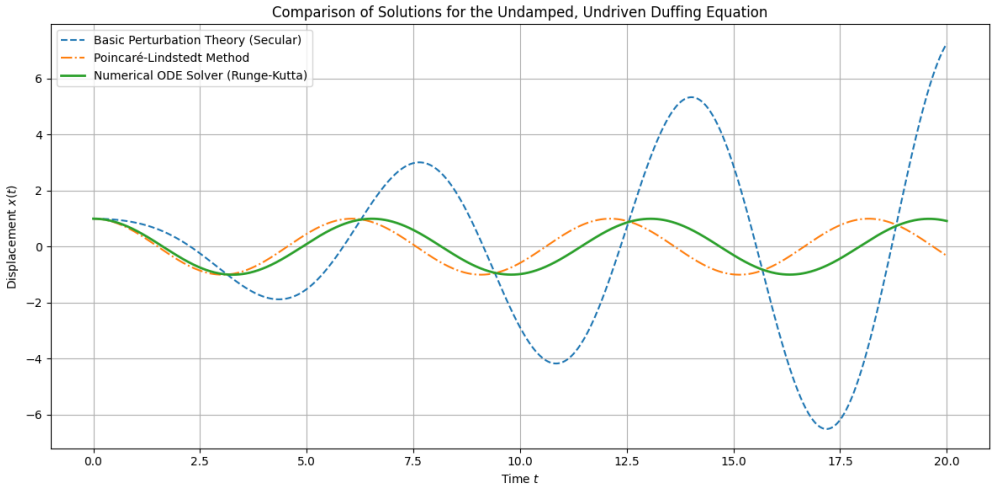

Figure 3: Comparison of solutions for the undamped, unforced Duffing equation. The blue dashed curve shows the basic perturbation theory (with secular growth), the orange dash-dot curve represents the Poincaré–Lindstedt solution, and the green solid curve is the numerical Runge–Kutta result.

Figure 3 shows a comparison of three approaches: the basic perturbation theory, the Poincaré–Lindstedt method, and a numerical solution computed via Runge–Kutta. The basic perturbation series initially tracks the reference curve but ultimately diverges because of the secular term proportional to $t\,\sin(\omega t)$. The Poincaré–Lindstedt method, by contrast, removes the resonant contribution at first order and retains a bounded behavior that remains close to the numerical trajectory for the entire duration of the simulation. The numerical solution is accepted as an accurate benchmark, given that energy conservation in the undamped, unforced regime is satisfied up to numerical precision.

However, it is observed that over extended periods, the frequency of the Poincaré–Lindstedt solution begins to deviate from that of the Runge-Kutta numerical solution. This deviation is expected and arises due to the inherent limitations of perturbative methods. The Poincaré–Lindstedt technique, while effective at eliminating secular terms and providing a bounded oscillatory solution, typically incorporates only a finite number of terms in the perturbative expansion. Consequently, higher-order nonlinear effects that accumulate over time are not fully captured, leading to a gradual divergence from the more exact numerical solution. Additionally, the first-order approximation in the Poincaré–Lindstedt method may not suffice for accurately describing the system's dynamics over long timescales, especially as the amplitude A or the nonlinearity parameter ϵ increases. To mitigate this, extending the perturbative expansion to higher orders can enhance the agreement with numerical solutions, although at the cost of increased analytical complexity. This behavior underscores the trade-off between analytical tractability and long-term accuracy in perturbative approaches.

Further insights into the system are gained by examining the phase diagram, which depicts the trajectory in the (x, v) plane. Each initial displacement A corresponds to a particular energy (assuming $m = 1$) according to

$$E \;=\; \tfrac{1}{2}\,v^2 + \tfrac{k}{2}\,x^2 - \tfrac{\epsilon}{4}\,x^4.$$

Because the total energy is conserved in the absence of damping and external forcing, the motion for any fixed energy traces out a closed loop.

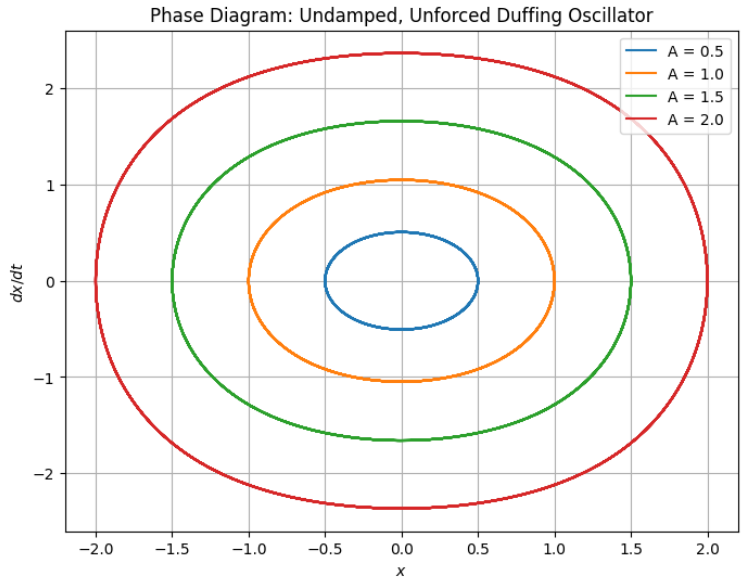

Figure 4: Phase diagram of the undamped, unforced Duffing oscillator for several initial amplitudes. Each curve corresponds to a distinct constant energy, yielding closed loops in the (x, v) plane. Larger energies result in broader loops, illustrating the system's bounded but amplitude-dependent oscillatory behavior.

Figure 4 illustrates how different initial amplitudes produce loops of varying size. Larger initial displacements lead to wider orbits, indicating higher total energy. No two loops intersect because the solution to the ordinary differential equation is unique for any given initial condition, and trajectories remain on their respective energy surfaces for all time. These closed loops confirm the bounded nature of the motion in the undamped, unforced case, agreeing with the conclusion that no secular growth should occur once the resonance is properly accounted for.

4 Chaotic Duffing Equation: Forcing, Damping, and Numerical Investigations

The Duffing system described thus far remains energy-conserving as long as no damping or external forcing is present. Once those terms are introduced, the equation takes the form (now we are switching back to a more standard form of the duffing equation)

$$\ddot{x}(t) \;+\; \delta\,\dot{x}(t) \;+\; \alpha\,x(t) \;+\; \beta\,x^3(t) \;=\; \gamma\cos(\omega\,t) \tag{15}$$

where $\delta > 0$ provides a dissipation proportional to velocity $\dot{x}(t)$, α and β are linear and cubic stiffness parameters, and the driving term $\gamma\cos(\omega t)$ injects energy at angular frequency ω. The coexistence of dissipation and forcing allows for a variety of steady-state behaviors, including regular limit cycles, period-doubled orbits, and chaotic attractors.

4.1 First-Order System Formulation

Just as in the undamped case, one can recast (15) into a pair of first-order equations by defining $v(t) = \dot{x}(t)$:

$$\dot{x}(t) \;=\; v(t), \quad \dot{v}(t) \;=\; -\,\delta\,v(t) \;-\; \alpha\,x(t) \;-\; \beta\,x^3(t) \;+\; \gamma\,\cos\!\big(\omega t\big)$$

For this set of equations there is no general closed-form solution for arbitrary choices of δ, α, β, γ, and ω. Consequently, one typically relies on numerical integration to probe the long-term behavior. In this project, as down in the previous sections, `solve_ivp`, a method from SciPy (with a Runge–Kutta integrator) is used to solve for $x(t)$ and $v(t)$ over different parameter sets.

4.2 Simulation Parameters and Graphing Strategy

To investigate how the driving amplitude γ influences transitions from periodic motion to chaos, a series of simulations is performed with the following fixed values:

$$\delta = 0.1, \quad \alpha = -1, \quad \beta = 1, \quad \omega = 1.4, \quad x(0) = v(0) = 0, \quad \Delta t = 0.1$$

Four distinct values of γ (0.1, 0.318, 0.338, and 0.35) are considered, each integrated over a designated time interval. Table 1 summarizes these choices, along with the intervals selected for full-time and zoomed-in plots. Each case includes two (or more) plots: the first covers the entire simulation interval, while the second focuses on a later time window to highlight the final state.

Table 1: Duffing Simulations: Driving Amplitudes γ and Time Intervals

Case	γ	Time Intervals for Plots
1	0.1	$[0, 200]$ and $[150, 200]$
2	0.318	$[0, 800]$ and $[789.85, 799]$
3	0.338	$[0, 2000]$ and $[1981.97, 2000]$
4	0.35	$[0, 3000]$, $[0, 300]$, $[2959.85, 3000]$, and $[2989.85, 3000]$

The rationale for these graphs is to observe how the system behaves initially (including transients) and to determine whether it settles into a periodic orbit, a period-doubled orbit, or an apparently chaotic trajectory over the long term.

4.3 Results for Increasing Driving Amplitudes

Case $\gamma = 0.1$. Figure 5 depicts the displacement $x(t)$ and velocity $v(t)$ over $t \in [0, 200]$. The initial oscillations gradually diminish in amplitude, and the solution converges to a regular, steady-state cycle. In the zoomed range $[150, 200]$ (Fig. 6), the motion is visibly periodic with a constant amplitude and a single period matching the driving frequency. The relatively weak driving force never exceeds the dissipation sufficiently to destabilize the system from its simple oscillation.

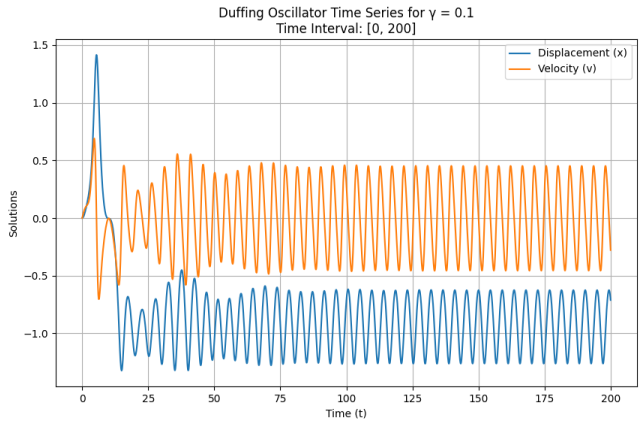

Figure 5: Time series for $\gamma = 0.1$, $t \in [0, 200]$. The displacement and velocity reach a single stable periodic orbit after the transient.

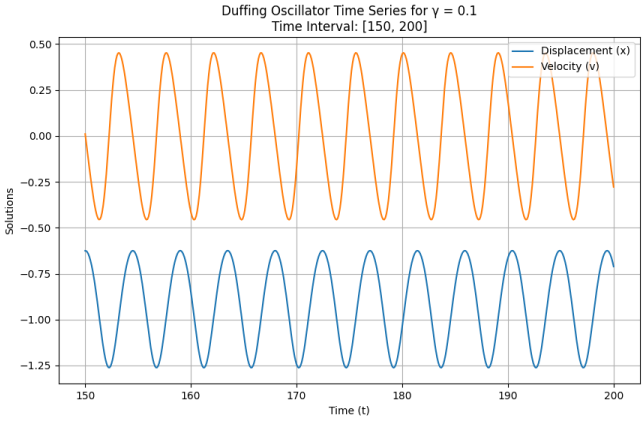

Figure 6: Zoomed view for $\gamma = 0.1$, $t \in [150, 200]$. The solution maintains a constant amplitude and phase relationship, reflecting a stable periodic motion.

Case $\gamma = 0.318$. At a higher driving amplitude, the system takes longer to settle and eventually demonstrates *period doubling*. Figure 7 shows the initial interval $[0, 200]$, where the motion is more irregular than in the $\gamma = 0.1$ case. Over the full integration to $t = 800$, the system adopts a cycle that completes every *two* drive periods rather than each single period. The zoomed time window $[789.85, 799]$ in Fig. 8 confirms the presence of two distinct oscillatory loops before the pattern repeats. This doubling of the fundamental period is a precursor to more complicated orbits and possible chaos.

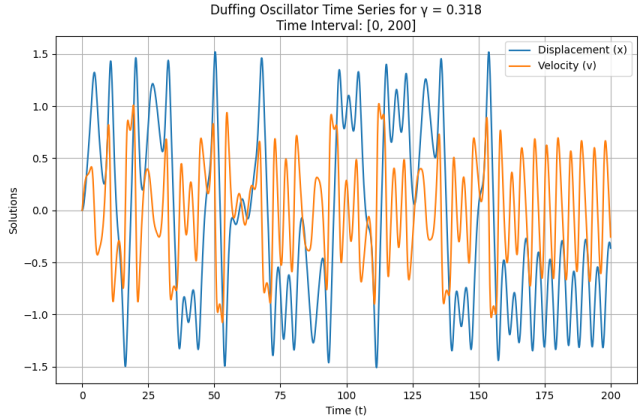

Figure 7: Time series for $\gamma = 0.318$, $t \in [0, 200]$. The amplitude evolves more intricately than in the lower-forcing case. Eventually, a period-doubled cycle appears.

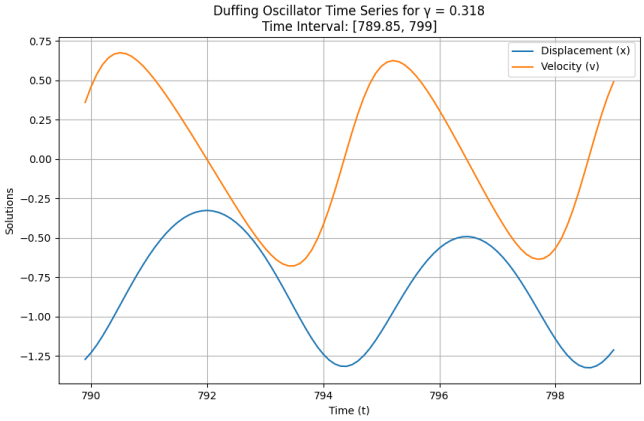

Figure 8: Zoomed view for $\gamma = 0.318$, $t \in [789.85, 799]$. Two oscillations occur for each driving cycle, illustrating a period-doubled orbit.

Case $\gamma = 0.338$. Further increments in γ push the system to additional bifurcations. Over a long integration to $t = 2000$, the oscillator transitions into a *four*-loop orbit (not pictured in a single figure, but visible within the project's code outputs). Figure 9 captures the first 200 time units, revealing complex amplitude modulations. In the later interval $[1981.97, 2000]$ (Fig. 10), the system exhibits four distinct maxima before repeating, indicative of another period-doubling event. Such cascades are a classical route to chaos in nonlinear oscillators.

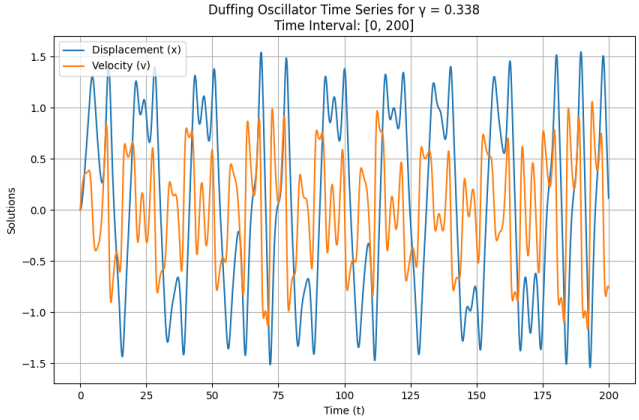

Figure 9: Time series for $\gamma = 0.338$, $t \in [0, 200]$. The motion evolves irregularly during this initial stage. Eventually, a quadruple-loop orbit emerges at long times.

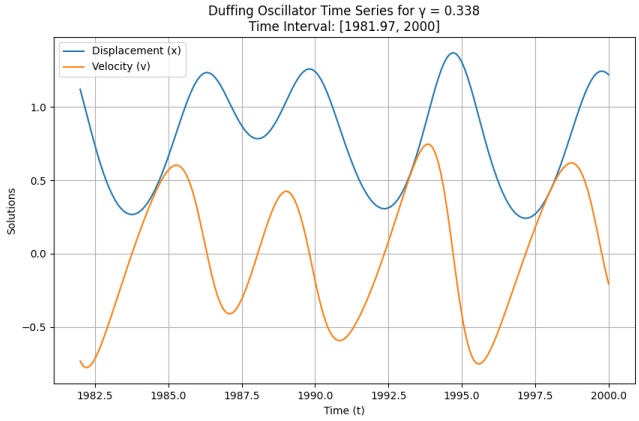

Figure 10: Zoomed view for $\gamma = 0.338$, $t \in [1981.97, 2000]$. Four peaks appear in each cycle, consistent with period-4 motion.

Case $\gamma = 0.35$. Once γ increases to 0.35, the oscillator no longer settles into any finite set of loops. Instead, the final motion is chaotic. Figure 11 shows $[0, 300]$, where the displacement and velocity already appear to fluctuate aperiodically. The subplots over $[2959.85, 3000]$ (Fig. 12) and $[2989.85, 3000]$ (Fig. 13) confirm that the trajectory does not return to a stable cycle; instead it continues to wander in an unpredictable manner. Small changes in initial conditions or parameters would yield markedly different paths, demonstrating sensitive dependence characteristic of chaos.

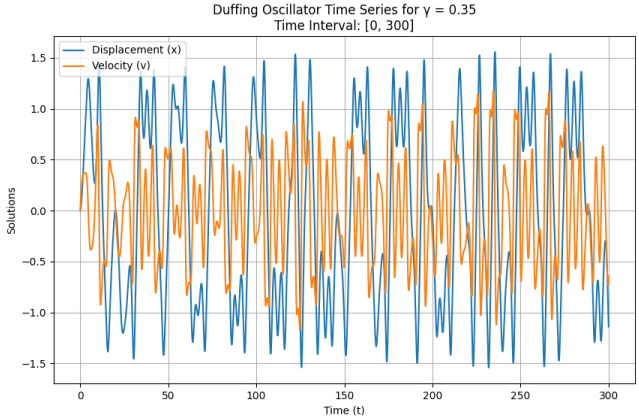

Figure 11: Time series for $\gamma = 0.35$, $t \in [0, 300]$. The system no longer exhibits a simple or multi-periodic motion and is indicative of chaos.

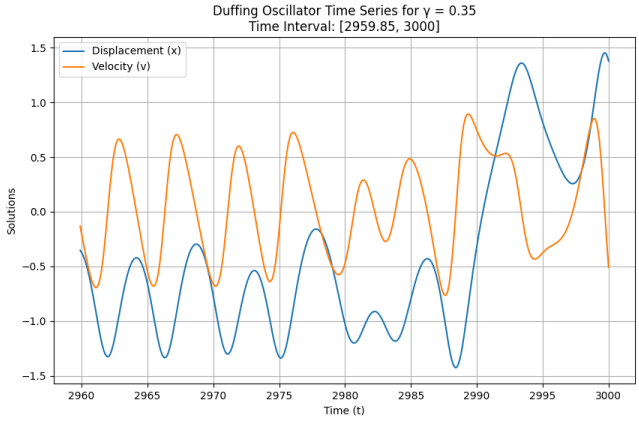

Figure 12: Focused interval $[2959.85, 3000]$ for $\gamma = 0.35$. The displacement and velocity vary erratically, with no single loop or repeating cycle.

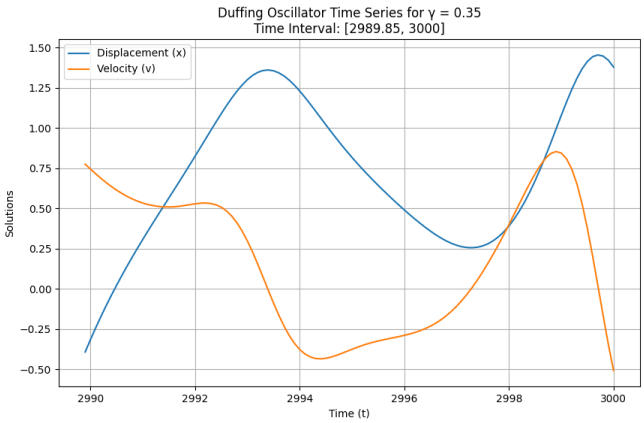

Figure 13: Further zoom into $[2989.85, 3000]$ for $\gamma = 0.35$. The motion remains aperiodic, illustrating the chaotic regime.

4.4 Interpretation and Transition to Chaos

These results demonstrate how gradually raising the forcing amplitude γ shifts the Duffing oscillator from a simple periodic response ($\gamma = 0.1$) to period-doubled orbits ($\gamma = 0.318$ and $\gamma = 0.338$), and ultimately to chaos ($\gamma = 0.35$). The interplay between damping and forcing, when mediated by the nonlinear stiffness terms, permits energy to accumulate or dissipate in such a way that multiple stable cycles can emerge or vanish. Period-doubling cascades are well-established gateways into chaotic dynamics, and the final parameter setting illustrates how even a modest change in γ can push the system into a chaotic attractor, with solutions that never settle into a repeating pattern and exhibit strong sensitivity to initial conditions.

5 Conclusion

This project has explored the Duffing oscillator in two major regimes: (1) the undamped and unforced case, and (2) the damped, forced case where chaos can arise. In the undamped setting, we showed that exact energy conservation yields a solution in terms of elliptic integrals, while standard perturbation expansions produce secular growth. The Poincaré–Lindstedt method circumvents such unbounded terms by adjusting the natural frequency at each order. Numerical solutions (Runge–Kutta) confirm that the Poincaré–Lindstedt expansion remains valid over long time intervals, but eventually higher-order effects accumulate. The phase-plane analysis reinforces the view that each trajectory is constrained to a particular energy surface, forming a closed orbit.

When damping and periodic forcing are introduced, energy balance is lost, and the system is driven by a combination of external energy input and internal dissipation. Numerical investigations at various forcing amplitudes γ reveal a progression: simple periodic oscillations give way to period-doubling and eventually to chaos. Small changes in γ can significantly alter the final attractor—from stable limit cycles to a fractal-like distribution of points in the phase plane. This transition underscores the hallmark of chaotic systems: strong sensitivity to initial conditions and the inability to predict long-term outcomes without precise knowledge of the initial state.

Overall, the Duffing equation provides an instructive example of how nonlinear terms in the restoring force can lead to phenomena ranging from amplitude-dependent oscillations in the undamped regime to period-doubling cascades and chaos in the damped, driven regime. Both an-

alytic methods (energy arguments, perturbation theory, Poincaré–Lindstedt, etc.) and numerical approaches (Runge–Kutta integrations, phase diagrams) form a complementary toolkit to understand and visualize the rich behavior of this classic nonlinear oscillator. Such methods and findings are directly transferable to broader contexts in classical mechanics, where many real-world systems deviate from purely linear laws and exhibit intriguing, sometimes chaotic, dynamics.

References

[1] G. Duffing, *Erzwungene Schwingungen bei veraenderlicher Eigenfrequenz und ihre technische Bedeutung*, Sammlung Vieweg, Braunschweig, 1918.

[2] S. H. Strogatz, *Nonlinear Dynamics and Chaos*, 2nd ed., Chapter 7: Perturbation Methods, Westview Press, 2018.

[3] Marian Thorten, *Classical Dynamics of Particles and Systems*, 5th ed., Chapter 4: Nonlinear Oscillations and Chaos, Cengage Learning, 2024.

A Additional Derivations

A.1 Detailed Solvability Condition and the Choice of Ω_1

After rewriting the Duffing equation

$$\ddot{x} + k\,x - \epsilon\,x^3 = 0$$

in terms of $\tau = \Omega\,t$, we obtain, to first order in ϵ,

$$\Omega^2 X_1''(\tau) + k\,X_1(\tau) \;=\; \epsilon\,X_0^3(\tau),$$

where $\Omega^2 = k + 2\,\omega\,\epsilon\,\Omega_1 + O(\epsilon^2)$ and $\omega = \sqrt{k}$. Collecting precisely the $\mathcal{O}(\epsilon)$ terms and dividing through by $\omega^2 = k$, one arrives at

$$\Big(k + 2\,\omega\,\epsilon\,\Omega_1\Big)X_1''(\tau) \;+\; k\,X_1(\tau) \;-\; \epsilon\,X_0^3(\tau) \;=\; 0$$

Writing $k = \omega^2$ and isolating the ϵ part on the right gives

$$\omega^2\,X_1''(\tau) + \omega^2\,X_1(\tau) \;=\; \epsilon\,X_0^3(\tau) \;-\; 2\,\omega\,\epsilon\,\Omega_1\,X_1''(\tau).$$

Divide by ω^2:

$$X_1''(\tau) + X_1(\tau) \;=\; \frac{\epsilon\,X_0^3(\tau)}{\omega^2} \;-\; \frac{2\,\omega\,\epsilon\,\Omega_1}{\omega^2}\,X_1''(\tau)$$

At $\mathcal{O}(\epsilon)$, we only need the homogeneous solution for X_1 plus a particular solution driven by known trigonometric terms. Recall that

$$X_0(\tau) \;=\; A\,\cos(\tau), \quad X_0^3(\tau) \;=\; A^3\cos^3(\tau) \;=\; A^3\Big[\tfrac{3\cos(\tau)+\cos(3\tau)}{4}\Big].$$

Thus,

$$\frac{X_0^3(\tau)}{\omega^2} \;=\; \frac{A^3}{4\,\omega^2}\Big[\,3\cos(\tau) + \cos(3\tau)\Big]$$

A resonance arises if a $\cos(\tau)$ term appears on the right-hand side *without* being canceled. However, the extra term

$$-\frac{2\,\omega\,\Omega_1}{\omega^2}\,X_1''(\tau)$$

can be chosen such that *remove* any net $\cos(\tau)$ forcing. More explicitly, we are looking for a "solvability condition" that ensures the coefficient of $\cos(\tau)$ is zero (which is one of the core techniques of this method).

Key matching step (essentially by inspection) We isolate the $\cos(\tau)$ portion. The coefficient in front of $\cos(\tau)$ from $A^3[3\cos(\tau)+\cos(3\tau)]/(4\omega^2)$ is $\frac{3A^3}{4\omega^2}$. Meanwhile, the $-\frac{2\omega\,\Omega_1}{\omega^2}X_1''(\tau)$ term must supply an offsetting $\cos(\tau)$. By comparing coefficients in the inhomogeneous equation at the resonance frequency $\tau \mapsto \cos(\tau)$, one finds the condition that

$$\boxed{\Omega_1 \;=\; \frac{3\,A^2}{8},}$$

Hence, by *choosing* Ω_1 in this way, no secular term (proportional to $t\,\sin(\tau)$) arises in $X_1(\tau)$. Therefore, to first order,

$$\Omega \;=\; \omega + \epsilon\,\Omega_1 \;=\; \sqrt{k} + \epsilon\,\frac{3\,A^2}{8},$$

and the solution

$$x(t) \;=\; A\,\cos\Big[\big(\omega + \epsilon\,\tfrac{3\,A^2}{8}\big)\,t\Big]$$

remains purely oscillatory without a growing (secular) component.